Chemical Engineering Journal 419 (2021) 129656

Contents lists available at ScienceDirect

Chemical Engineering Journal

journal homepage: www.elsevier.com/locate/cej

Cu-ZrO_2 catalysts with highly dispersed Cu nanoclusters derived from ZrO_2@ HKUST-1 composites for the enhanced CO_2 hydrogenation to methanol

Jiahui Yu [a,b], Shuai Liu [a,b], Xueliang Mu [c], Gang Yang [a,b], Xiang Luo [a,b], Edward Lester [d], Tao Wu [a,b,*]

[a] Department of Chemical and Environmental Engineering, University of Nottingham Ningbo China, Ningbo 315100, China
[b] Key Laboratory of Carbonaceous Wastes Processing and Process Intensification of Zhejiang Province, University of Nottingham Ningbo China, Ningbo 315100, China
[c] Department of Mechanical and Energy Engineering, Southern University of Science and Technology, Shenzhen 518055, China
[d] Department of Chemical and Environmental Engineering, The University of Nottingham, Nottingham NG7 2RD, UK

ARTICLE INFO

Keywords:
Cu nano-cluster
CO_2 hydrogenation
DFT simulation
Cu-ZrO_2 interfaces

ABSTRACT

In this study, a series of Cu-ZrO_2 catalysts with highly dispersed Cu nanoclusters were prepared via the calcination and reduction of ZrO_2@HKUST-1 precursors. These catalysts demonstrated an outstanding selectivity in the yield of methanol during CO_2 hydrogenation. The space-time yield (STY) of methanol is 5.2 times higher than that of those similar catalysts reported by other researchers, which were prepared using conventional method and tested under the same testing conditions. Density functional theory (DFT) study revealed that the activation of CO_2 occurs at the Cu-ZrO_2 interfaces and facilitates the hydrogenation of CO_2 to methanol. It is concluded that the controlled formation of the highly dispersed Cu nanoclusters not only provides a large number of highly efficient active centers for CO_2 hydrogenation, but also leads the generation of more Cu-ZrO_2 interfaces. These two effects contribute to the superior catalytic performance of the nano Cu-ZrO_2 catalyst in CO_2 hydrogenation.

1. Introduction

Carbon dioxide is one of the greenhouse gases that have led to severe global warming. Theoretically, CO_2 can be converted into methanol, a basic organic chemical raw material that is widely used as a feedstock in organic synthesis, pharmaceutical industry as well as an alternative fuel [1,2]. In the past two decades, a significant amount of effort has been made to convert CO_2 into chemicals and fuels aiming at the mitigation of CO_2 emission, which include the hydrogenation of CO_2 to produce methanol as a hot topic for research.

Copper-based catalysts have been widely used in industrial-scale methanol synthesis [3–5]. It is reported that the activity of copper-based catalysts is dependent on the dispersion of Cu nanoclusters on the support [6,7], while the size of Cu nanoclusters also shows a strong correlation to its catalytic performance [8,9]. In recent years, the effects of highly dispersed Cu nanoclusters on catalytic performance have been studied extensively [10,11]. A recent study showed that the decrease in the Cu particle size from 28 nm to 6.5 nm could lead to the increase in the CO_2 conversion from around 2.5 to 10.7% [12]. However, small Cu nanoclusters can easily form large particles (with a lower catalytic activity) during the course of preparation when they are exposed to relatively high temperatures [13]. Therefore, it is of great importance to develop novel preparation methods that enable the formation of highly dispersed Cu nanoclusters on the support.

Generally, metal-support interfaces have unique properties and play an important role in catalysis [14–16]. Scholars have found that the hydrogenation reaction occurs at the interface of CeOx/TiO_2 [17] and the rate of CH_3OH formation increases with the Cu/Al_2O_3 interface [18]. It is also reported that the Cu/ZnO interfaces are the active sites dictacting CH_3OH selectivity [19]. Thus, it is worthwhile studying the roles of the metal-support on the yield and selective formation of CH_3OH during CO_2 hydrogenation.

In this study, a new method was developed for the preparation of Cu-ZrO_2 catalysts to control the formation of Cu nanoclusters on the support and its dispersion aiming at enhancing the catalytic hydrogenation of CO_2 to methanol. The HKUST-1 serves as the copper enabling the formation of highly dispersed Cu nanoclusters on the ZrO_2 surface after calcination. These catalysts were studied extensively to reveal their

* Corresponding author at: Department of Chemical and Environmental Engineering, University of Nottingham Ningbo China, Ningbo 315100, China.
E-mail address: tao.wu@nottingham.edu.cn (T. Wu).

https://doi.org/10.1016/j.cej.2021.129656
Received 23 December 2020; Received in revised form 27 March 2021; Accepted 31 March 2021
Available online 7 April 2021

catalytic performance in CO_2 hydrogenation to methanol. Moreover, DFT calculations were carried out to study the reaction pathways and the formation of products and by-products.

2. Experimental

2.1. Preparation of catalysts

2.1.1. Polyvinylpyrrolidone (PVP)-stabilized ZrO_2 nanoparticles

The polyvinylpyrrolidone(PVP)-stabilized ZrO_2 nanoparticles were synthesized following the procedure described elsewhere [20]. Approcimmately 0.5 g of zirconia (20 nm, 99.99% purity, supplied by Shandong Xinya chemical reagent) was initially dispersed in 500 mL ethanol, treated ultrasonically for 3 h, and then filter by 220 nm filter paper, stirring for 10 min at room temperature in a round bottom flask. Around 0.5 g of PVP solution (molecular weight around 4,000 g mol^{-1}) was then slowly added to the well-dispersed zirconia-ethanol suspension under continuous stirring and was refluxed under continuous stirring for another 2 h. The PVP-stabilized ZrO_2 NPs were collected by centrifugation at 6,000 rpm for 3 min, washed by ethanol for three times, and then dispersed in ethanol (0.5 mg mL^{-1}).

2.1.2. Synthesis of ZrO_2@HKUST-1 core–shell precursor

A series of ZrO_2@HKUST-1 composites were prepared in an autoclave, which were labelled as × % ZrO_2@HKUST-1, where × % represents the weight percentage of HKUST-1. In a typical experiment, the pre-determined amount of poly (N-vinyl-2-pyrrolidone) (PVP)-stabilized ZrO_2 nanoparticles suspension (0.5 mg mL^{-1}) was mixed with ethanolic solution of copper nitrate (0.181 g) and trimesic acid (0.105 g) and was kept isothermal at 120 ℃ for 12 h in the autoclave. The mixture was then washed with methanol at 80 ℃ for 3 h, followed by centrifugation at 6000 rpm for 3 min to remove the excessive reactant. The ZrO_2@HKUST-1 composite was obtained after drying at 120 ℃ in an oven.

2.1.3. Preparation of Cu-ZrO_2 catalyst

It was prepared by the calcination of ZrO_2@HKUST-1 composites at 320 ℃ for 4 h in air, followed by the reduction in 10% H_2/Ar for 1 h at 300 ℃. The catalysts are labelled as × %Cu-ZrO_2, where × represents the weight percentage of copper. The 3, 12, 24, 42 wt%Cu-ZrO_2 catalysts were derived from 10, 30, 50, 70 wt% ZrO_2@HKUST-1 precursor respectively.

To further demonstrate the effect of calcination, the gas flow was change from air alone for 4 h to Y (Y < 4) h in N_2 followed by (4-Y) h in air. The catalysts were denoted as × % Cu-ZrO_2-Y-(4-Y). For instant, 12% Cu-ZrO_2-2–2 represents a catalyst that contains 12 wt% copper and is calcined in N_2 for 2 h before 2 h in air at 320℃.

2.1.4. Synthesis of Cu-ZrO_2-im composites

It was prepared by immersing of copper nitrate in ZrO_2 suspension in the same composition then calcined under the same condition as a control group, which were labelled as × % Cu-ZrO_2-im.

2.2. Characterization of catalysts

The morphology and structure of the samples (before and after calcination) were studied using SEM (Zeiss Sigma VP) and TEM (JEM2100). Nitrogen adsorption was performed to determine specific surface area using a Micromeritics Tristar 3020, following the procedure described elsewhere [21,22]. Prior to testing, the sample was degassed at 150 ℃ for 12 h. Powder X-ray diffraction (XRD) patterns were obtained using Bruker D8 A25 diffractometer between 5 $^o2\theta$ and 90 $^o2\theta$ with CuKα radiation.

Temperature-Programmed H_2 reduction (H_2-TPR), Temperature-Programmed CO_2 desorption (CO_2-TPD), Temperature-Programmed H_2 desorption (H_2-TPD) and metal dispersion tests were carried out using a BELCAT II (MicrotracBEL).

During the H_2-TPR, approximately 30 mg of sample was flushed with He for 15 min before being heated from 50 to 600 ℃ in 5 vol% H_2 + 95 vol% Ar at a flow rate of 30 mL min^{-1}, with the detailed procedure described elsewhere [23].

During the CO_2-TPD, approximately 50 mg of sample was heated to 120℃ for 15 min in He to remove the trapped water then cooling down to room temperature. The sample was subsequently heated to 250 ℃ and purged for 60 min with H_2 at a flow rate of 30 mL min^{-1} to fully reduce the catalysts. After being cooled to room temperature, the samples were purged with CO_2 for 60 min at 50 ℃ to saturate the surface of the catalyst. The TPD program was performed across a temperature range of 50–600 ℃ at a heating rate of 10 ℃ min^{-1}. The details of CO_2-TPD process can be found in literature [23].

Copper dispersion test were conducted by a typical TPR-N_2O-TPR method [9]. First, 50 mg samples was purged with Ar at 200 ℃ for 1 h and then cooling down to room temperature. Then switch the gas to H_2(5%vol.)/Ar. After the baseline stabilizes, the temperature was increased to 350 ℃ at 10 ℃ min^{-1}. The amount of hydrogen consumption in the first TPR was denoted as A_1. After being reduced, the sample was cooled to 60 ℃. Then the gas was switched to N_2O gas with a flow rate of 30 mL/min, and was kept for 1 h, followed by the gas switched to Ar to flush out the oxidant and cooled to room temperature and then start another TPR. Hydrogen consumption in the second TPR was denoted as A_2. The copper dispersion and exposed copper surface area [9] were calculated based on Van Der Grift's equation [24]:

Metal dispersion [percentage of metal surface exposure]: D_m(%)

$$D_m = 2A_2/A_1 \times 100\% \quad (1)$$

Exposed Cu surface area: Scu(m^2-Cu/g-Cu)

$$S_{Cu} = 2A_2 \times N_{av}/(A_1 \times M_{Cu} \times 1.47 \times 10^{19}) \approx 1353 \times \frac{A_2}{A_1} \quad (2)$$

where *N*av = Avogadro's constant, *M*Cu = relative atomic mass (63.456 g mol^{-1}), Copper atoms surface density(1.47×10^{19} atom m^{-2})

Average volume-surface diameter can be calculated using following equation [9]:

$$d_{Cu} = \frac{6}{S_{Cu} \times \rho_{Cu}} \approx 0.5\frac{A_1}{A_2} \quad (3)$$

where, ρCu is the density of copper (8.92 g cm^{-3}).

Eyring equation:

$$k = \frac{k_B T}{h} e^{-\Delta G/k_B T} \quad (4)$$

Where Δ G is Gibbs Free Energy (cal mol^{-1}); h is Planck constant; T is Temperature (K); and K_B is Boltzmann constant.

$$TOF = \frac{\mu_{CO_2} \times X_{CO_2} \times M_{Cu}}{V_m \times \omega_{Cu} \times m_{cat} \times d_{Cu}} \quad (5)$$

where μCO_2 is CO_2 flow rate in the feed gas, X_{CO2} refers to CO_2 conversion, M_{Cu} is copper molar mass, V_m is the standard molar volume, ω_{Cu} is copper mass percentage in the catalyst, m_{cat} is the amount of the catalyst used, and D_{Cu} is the copper dispersion.

2.3. Evaluation of catalytic performance

The performance of catalysts was evaluated using a fixed-bed microreactor under an elevated pressure [25]. Firstly, the catalyst (200 mg, diluted with 400 mg quartz sand) was pretreated in 5 %H_2/Ar at 300 ℃ for 1 h. After the catalyst was cooled down to room temperature under Ar. The test was conducted at a pressure of 3.0 MPa and a GHSV of 15000 mL $g^{-1}\cdot h^1$ in a temperature range of 200 to 280℃. The inlet gas mixture was of a molar ratio of H_2/CO_2/ Ar = 72:24:4. The exit gas was maintained over 90 ℃ under the protection of heating tape and was

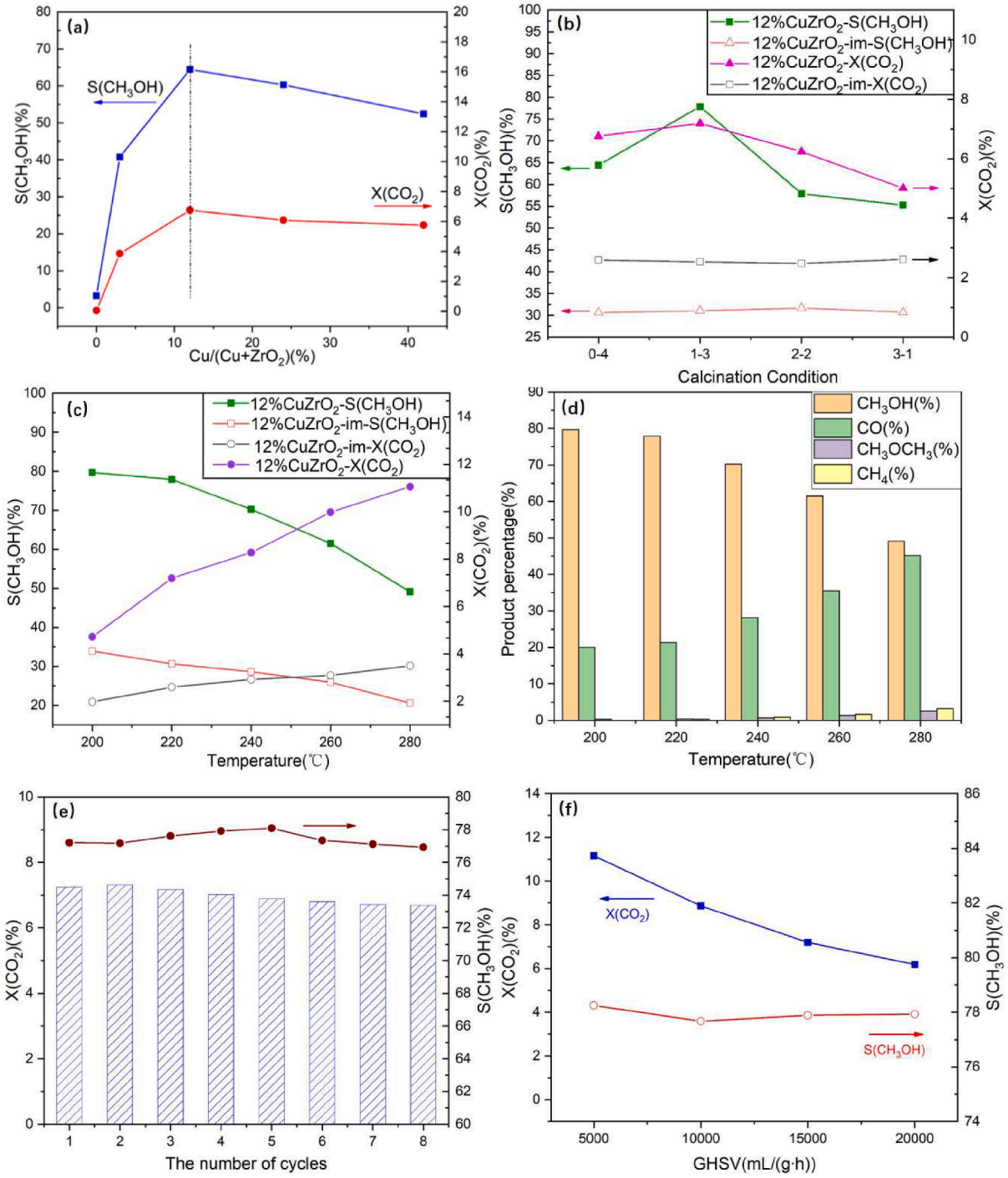

Fig. 1. (a) Dependence of catalytic performance on Cu/Cu + ZrO_2 weight ratio. (b) Influence of calcination method on the selectivity and conversion of CO_2. Temperature effects on (c) the conversion of CO_2 and the selectivity of CH_3OH of the 12% Cu-ZrO_2-1-3 catalyst, (d) the product of the 12%Cu-ZrO_2-1-3 catalyst under the pressure of 3 MPa and temperature between 220 ℃ with 280 ℃. (e) The stability test for the 12% Cu-ZrO_2-1-3 catalyst for 8 cycles. (f) Catalytic performance of the 12% Cu-ZrO_2-1-3 catalyst under different GHSV(mL g^{-1}·h^{-1}). Testing conditions: 220 ℃ and 3 MPa.

continuously analyzed using a mass spectrometer (Pfeiffer Thermo-Star GSD 320).Data were collected at the reaction time reaching 60 min (TOS = 60 min). The CO_2 conversion, X(CO_2), the carbon-based selectivity, S(product), and the space time yield of methanol, STY(CH_3OH), were calculated using the equations shown below.

$$X(CO_2) = \frac{[CO]_{out} + [CH_3OH]_{out} + [CH_4]_{out} + 2[CH_3OCH_3]_{out}}{[CO_2]_{in}} \quad (6)$$

$$S(CH_3OH) = \frac{[CH_3OH]_{out}}{[CO]_{out} + [CH_4]_{out} + [CH_3OH]_{out} + 2[CH_3OCH_3]_{out}} \quad (7)$$

$$S(CO) = \frac{[CO]_{out}}{[CO]_{out} + [CH_4]_{out} + [CH_3OH]_{out} + 2[CH_3OCH_3]_{out}} \quad (8)$$

$$STY(CH_3OH) = \frac{GHSV}{22.4} \times V\%(CO_2) \times X(CO_2) \times S(CH_3OH) \times M_{CH_3OH} \quad (9)$$

Table 1
Comparison of TOF and space time yield of methanol with reported papers.

Catalyst	Cu content (wt%)	Temperature (K)	Pressure (MPa)	TOF ($10^{-3}s^{-1}$)	STY (methanol) ($mg\cdot g^{-1}\cdot h^{-1}$)	Reference
$Cu_1La_{0.2}$/SBA-15	8.1	513	5.0	7.1	243.6	[34]
$CuZnOAl_2O_3ZrO_2$	50.1	463	5.0	7.3	87	[12]
Cu-ZnO-ZrO_2	38.2	503	5.0	–	160	[38]
Cd_aZrO_x	–	573	2.0	–	Circa 355	[36]
CuZnZrMgAl	10	543	2.8	1.0	121.5	[35]
Cu-ZnO-ZrO_2	45	513	3.0	–	140	[39]
Cu-ZnO-ZrO_2	36.2	493	3.0	9.8	297[1]	[32]
Cu-ZrO_2	46.4	493	3.0	2.0	46.2	[32]
Cu-ZrO_2	10	493	3.0	–	Circa 55	[37]
Cu-ZrO_2	11	493	3.0	4.5	287.9	This work

2.4. DFT modeling

DFT calculations were performed using VASP 5.4.4. The projector augmented wave (PAW) method was used with a plane wave energy cut-off of 500 eV [26]. The criterion for the convergence of the SCF cycle was chosen as 10^{-4} eV, and the optimization process was assumed to converge when the forces on all atoms were lower than 0.05 eV/Å.

The surface of monoclinic zirconia was chosen as (−111), the most abundant crystallographic planes in TEM and XRD. The slab was 13.5 Å (length) × 14.3 Å (width) × 8.5 Å (thickness) and 96 atoms, 32 ZrO_2 units) with a vacuum separation of 11.5 Å. The lowest atomic layers were fixed in the optimization and in the transition state calculations. The Brillouin zone was sampled with a 1x1x1 k-point grid.

The study of transition states were conducted using the Climbing Image Nudge Elastic Band (CI-NEB) method with 4 images, and was further confirmed by frequency analysis.

The Gibbs free energy was calculated by using the VASPKIT post-processing tool [27]. The vibration frequencies for all states, including the gas-phase molecules, the adsorbed species and the transition states were also determined.

3. Results and discussion

3.1. Catalysts activity

CO_2 hydrogenation on the as-prepared catalysts was performed to evaluate the catalytic performance in a temperature range of 200–280 °C under 3 MPa at a GHSV of 15000 mL/(g·h). Catalytic performance of the Cu-ZrO_2 catalysts with different Cu loadings is shown in Fig. 1(a). The m-ZrO_2 (denoted as 0 in copper percentage) showed a very low activity in methanol synthesis. However, the methanol yield varies significantly with Cu loading in Cu-ZrO_2. The highest CO_2 conversion (6.76%) and the highest methanol selectivity (64.4%) was found with the 12%Cu-ZrO_2 catalyst, which represents the best copper percentage among the catalysts investigated. Fig. 1(b) shows the CO_2 hydrogenation performance of catalysts prepared using different calcination methods. With the increase in calcination time (in nitrogen atmosphere) from 0 to 3 h, the conversion of CO_2 increased from 6.8 to 7.2% and then decreased to 5.0%. More importantly, a remarkable increase in methanol selectivity also occurred for 12% Cu-ZrO_2-1-3 (77.9%), which is about 1.2 times of that of the initial 12%Cu-ZrO_2-0–4 catalysts. It indicates that 12%Cu-ZrO_2-1-3 was the best catalyst with the highest STY of methanol (287.9 $mg\cdot g^{-1}\cdot h^{-1}$), as shown in Fig. S7.

In order to compare with the performance of the HKUST-1 derived catalysts, a standard Cu-ZrO_2-im catalyst with the same amount of copper was prepared using a traditional impregnation method, the performance of which is shown in Fig. 1(b). In general, both methanol selectivity and carbon dioxide conversion of 12%Cu-ZrO_2 were remarkably higher than that of 12%Cu-ZrO_2-im under the same reaction conditions, suggesting that the Cu-ZrO_2 prepared by the pyrolysis of ZrO_2@HKUST-1 composites helps improve the catalytic activity. It is worth noting that CO_2 conversion of 12%Cu-ZrO_2-1-3 is about 2.8 times higher than that of the 12%Cu-ZrO_2-im-1-3, and methanol selectivity increased from 31% for 12%Cu-ZrO_2-im-1-3 to 77.8% for 12%Cu-ZrO_2-1-3. Moreover, the space–time yield of methanol increased by 7.1 times (Fig. S7). It is also found that calcination atmosphere showed no impacts on catalytic performance for 12%Cu-ZrO_2-im catalysts, suggesting that the controllable interface effects only occur in the HKUST-1 derived catalysts.

The effects of reaction temperature on products distribution were performed as shown in Fig. 1(c,d). With the increase in temperature, the conversion of CO_2 increases, whereas the methanol selectivity decreases, which is consistent with literature [28,29]. It is believed that methanol synthesis and the reverse water–gas (RWGS) are the two parallel but competing reactions, as shown below:

$$CO_2 + H_2 \rightleftharpoons CH_3OH + H_2O \quad \Delta H^{\theta}_{298K} = -49kJ\cdot mol^{-1} \tag{R1}$$

$$CO_2 + H_2 \rightleftharpoons CO + H_2O \quad \Delta H^{\theta}_{298K} = 41kJ\cdot mol^{-1} \tag{R2}$$

$$CO + 2H_2 \rightleftharpoons CH_3OH \quad \Delta H^{\theta}_{298K} = -90kJ\cdot mol^{-1} \tag{R3}$$

Thermodynamically, the formation of methanol via R. (1) and R. (2) are exothermic, whereas the RWGS reaction is endothermic. As a result, increasing reaction temperature promotes the RWGS reaction, but hinders the formation of methanol.

The effect of reaction temperature on product yield is shown in Fig. 1 (d). With the elevation of reaction temperature, the percentage of carbon monoxide, methane and dimethyl ether (DME) increases. The reaction for the formation of DME and methane are shown in R. (4) and R. (5). DME and methane are the by-products [30]. Therefore, the presence of methane and DME as by-products indicates the occurrence of reverse water–gas (RWGS) and methanol formation from CO, and CO is an intermediate during methanol synthesis.

$$2CO_2 + 6H_2 \rightleftharpoons CH_3OCH_3 + 3H_2O \quad \Delta H^{\theta}_{298K} = -123kJ\cdot mol^{-1} \tag{R4}$$

$$CO_2 + 4H_2 \rightleftharpoons CH_4 + 2H_2O \quad \Delta H^{\theta}_{298K} = -165kJ\cdot mol^{-1} \tag{R5}$$

The stability of the 12%Cu-ZrO_2-1-3 is shown in Fig. 1(e) for 8 cycles. The CO_2 conversion is maintained at around 7% with a slight decrease. The methanol selectivity is maintained between 76 and 78% in the 8 cycles, which account for around 16 h testing. Considering that the high temperature agglomeration of copper-based catalysts is a common problem, this result is acceptable. The catalytic performance under different GHSV are also provided in Fig. 1(f). As shown in the Fig. 1(f), the conversion of CO_2 reduces with the increase of GHSV, which is caused by the unsaturated contact time between the reaction gas and the catalyst. The selectivity of methanol is kept at around 78% with small fluctuations. The result suggests that the contact time between the catalyst and the reactants greatly affects the carbon dioxide conversion, but it has little effect on the selectivity of the main product. This is in consistent with what was reported by Dongfang Wu and co-workers [31].

Table 1 compares the TOF values and the space time yield of methanol reported by other researchers. The TOF is an important indicator to

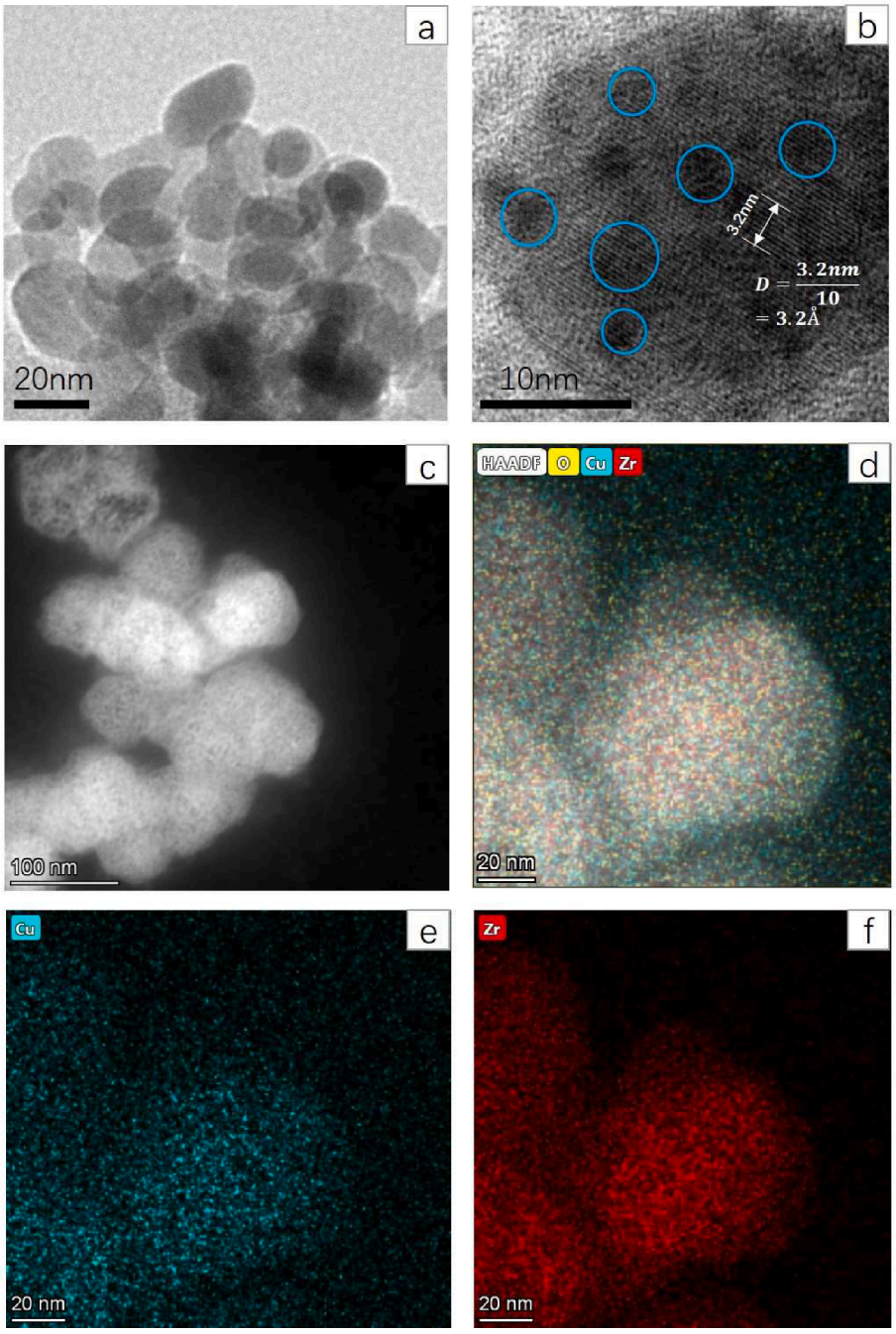

Fig. 2. TEM (a,b) and HAADF-STEM (c,d) images and elemental mappings (e,f) of 12%Cu-ZrO_2-1-3 catalysts.

show the catalytic activity of single active site [32,33]. The TOF value of the prepared 12%Cu-ZrO_2-1-3 catalyst is 4.5×10^{-3} s^{-1}, which is not as high as some published papers [12,34], but higher than others [32,35]. Although the single site catalytic ability of the prepared catalysts is not very high, its methanol producibility is high because the well dispersed copper leads to the formation of more active sites. It can also be seen in Table 1 that the solid solution catalyst [36] has a high catalytic activity with an STY of methanol of 355 $mg \cdot g^{-1} \cdot h^{-1}$. However, the catalyst required the use of cadmium which is highly toxic and an operating temperature as high as 573 K. Cu-ZnO-ZrO_2 on PMMA was found to be an effective catalyst for CO_2 hydrogenation to methanol with a STY (methanol) of 297 $mg \cdot g^{-1} \cdot h^{-1}$ [32]. However, the presence of ZnO is essential in the composites to promote the adsorption of CO_2. Without a ZnO promoter, the STY of methanol decreases significantly to 46.2 $mg \cdot g^{-1} \cdot h^{-1}$ and the selectivity drops to 58.7% under the same reaction conditions [32]. A similar study using Cu-ZrO_2 as the catalyst for CO_2 hydrogenation only led to a STY of methanol of approximately 55 $mg \cdot g^{-1} \cdot h^{-1}$ at 493 K and 3.0 MPa [37]. Herein, under the same operating conditions, the as-prepared Cu-ZrO_2 catalysts reached a methanol yield of 287.9 $mg \cdot g^{-1} \cdot h^{-1}$. This enhanced STY is attributed to the modification of the copper-zirconia interface via the formation of Cu nanoclusters without the need to add ZnO as a promoter, which is an advantage over Cu-ZnO-ZrO_2.

3.2. Surface characterization of the prepared catalysts

Researchers have discovered that Cu nanoclusters can significantly promote the catalytic performance [34,35]. The nano-catalysts derived

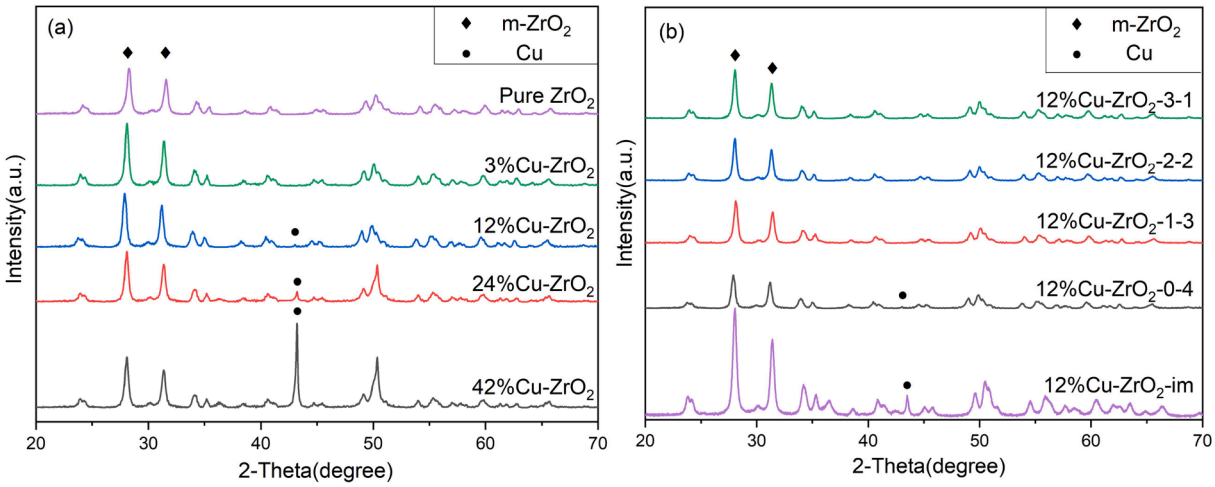

Fig. 3. (a) XRD patterns for as-prepared catalysts with different Cu contents; (b) the profiles of Cu-ZrO_2 catalysts prepared via different methods with a constant Cu-loading of 12%.

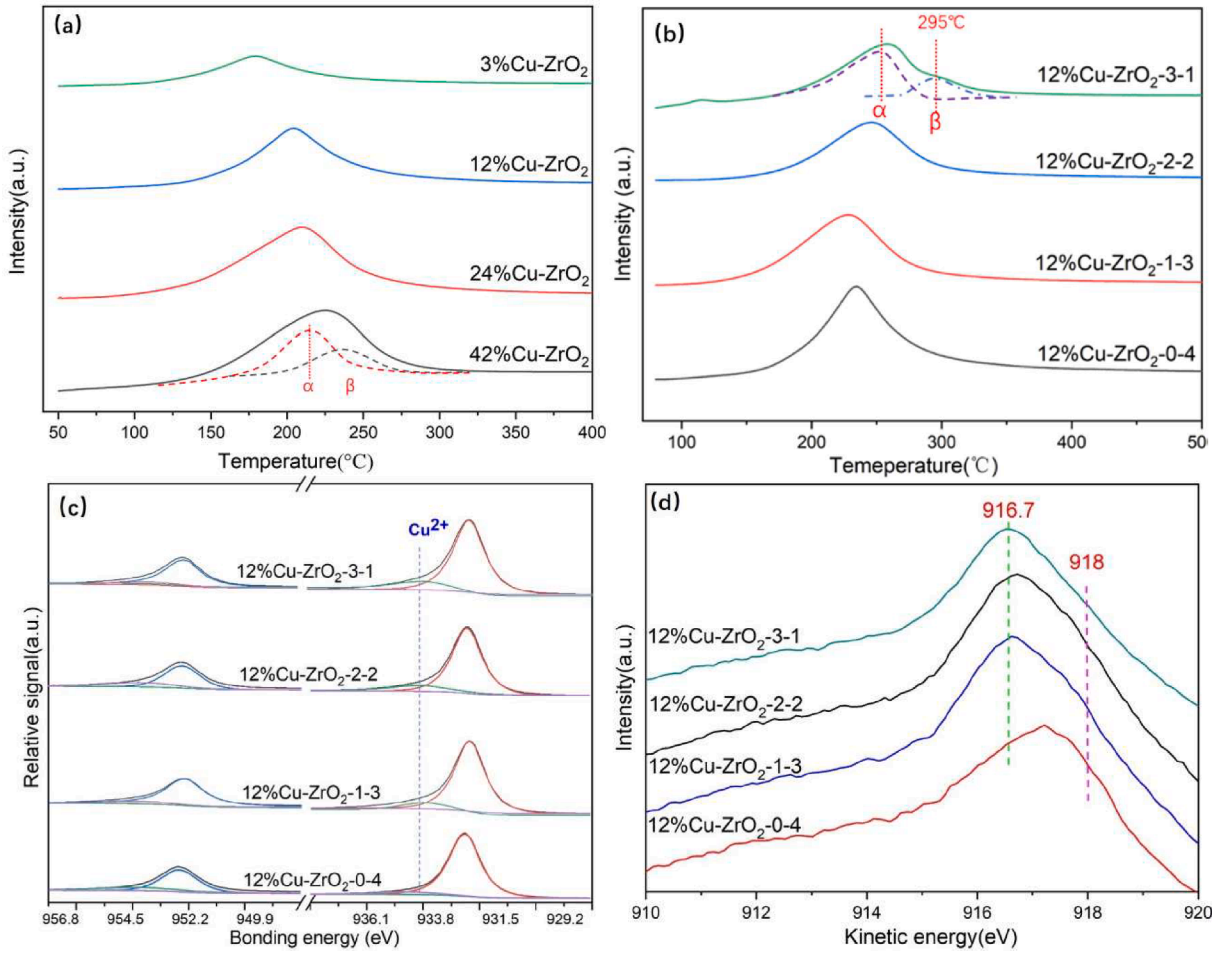

Fig. 4. TPR profile of (a) Cu-ZrO_2 catalysts with different components, and (b) 12%Cu-ZrO_2 catalysts with different calcination methods; (c) Cu 2p XPS spectra and (d) Cu Auger peaks of 12% Cu-ZrO_2 catalysts in different calcination methods.

from ZrO_2@HKUST-1 composites are characterized by HRTEM/mapping, XRD and XPS, as shown in Figs. 2–4. The characterization of the ZrO_2@HKUST-1 precursor is shown in Figs. S8–S11.

The morphology of the 12%Cu-ZrO_2-1-3 catalyst is shown in Fig. 2 using both TEM and HAADF-STEM. Fig. 2(a) shows that the particle size of the as-prepared catalyst was around 20 nm. Fig. 2(b) shows the presence of small black dots on the surface of 20-nm spheres with distinct crystal lattice under a higher magnification image scale. The (−111) planes of the sphere confirmed that the particles are zirconia. Moreover, the presence of copper was confirmed by EDS analysis (Fig. S16) and suggests that the blank dots are copper clusters. Similar particles have been reported by other researchers and confirmed to be

Table 2
Summary of copper dispersion, particle size and BET surface area.

Catalyst	Copper content (%)	Dcu (wt %)[b]	Scu [b] (m^2/g-Cu)	Scu [b] (m^2/g_{cat})	d_{Cu} (nm)[b]	BET (m^2/g)	Pore Volume (cm^3/g)
12%Cu-ZrO_2-im	11.43	7.1	48	5.8	14.1	25	0.04
3%Cu-ZrO_2	2.75	40.1	271	8.1	2.5	28	0.05
12%Cu-ZrO_2	11.02	29.3	198	23.7	3.4	32	0.05
24%Cu-ZrO_2	22.93	14.1	95	22.8	7.1	36	0.06
42%Cu-ZrO_2	41.27	7.7	52	21.8	13.0	23	0.04
12%Cu-ZrO_2-1-3	11.16	32.4	219	26.3	3.1	53	0.06
12%Cu-ZrO_2-2-2	11.09	31.6	214	25.7	3.2	67	0.10
12%Cu-ZrO_2-3-1	11.13	25.7	174	20.9	3.9	35	0.06

[a]Results from ICP-OES
[b] Calculated from N_2O surface oxidation.

metal clusters [40,41]. In Fig. 2(b), the copper clusters appear to be in the size between 3 and 5 nm, which is consistent with copper particles calculated from N_2O surface oxidation (3.1 nm). HAADF-STEM images and elemental mappings are the typical method to show the spatial distributions of elements [42]. In Fig. 2(d-f), the elemental mapping further confirmed the well-dispersed copper particles on the zirconia surface. These smaller copper clusters may contribute to the higher metal dispersion and more copper-zirconia interfaces. The copper, in the form of nano clusters, could increase the copper-zirconia interface and thus lead to a better catalytic performance. These results are also in line with the H_2-TPR and metal dispersion results, implying that the pyrolysis in nitrogen improves the dispersion of copper.

Fig. 3(a) shows the XRD figure of catalysts prepared with different copper contents. The pattern shows peak intensity changing with a higher level of copper ratio but no difference in overall peak position. There is little evidence of a copper peak for the 3%Cu-ZrO_2 catalyst, which may be attributed to the small percentage of copper. For the 24% Cu-ZrO_2 catalyst and the 42%Cu-ZrO_2 catalyst, there is an obvious peak at 43.3° corresponding to copper. However, the peak at 43.3° for the 12%Cu-ZrO_2 is not obvious, which may be due to the low level of copper crystallinity.

In Fig. 3(b), the peak at 43.3° disappears for the catalysts calcinated in nitrogen for 1–3 h. When compare 12%Cu-ZrO_2-1-3 with 12%Cu-ZrO_2-im, there is an obvious peak at 43.3° corresponding to Cu^0 for 12% Cu-ZrO_2-im but no peak for 12%Cu-ZrO_2-1-3. This suggests that for the Cu-ZrO_2 catalysts prepared via the normal impregnation method, the copper particles crystallize into large particles, whereas for 12%Cu-ZrO_2-1-3, the copper particles are well dispersed on the support and are difficult to be detect by XRD. It suggests that the calcination in nitrogen could prevent copper nanoclusters from forming larger particles.

Table 2 summarized copper dispersion information and BET surface area of the as prepared catalysts. When the copper content is 3 wt%, the copper dispersion of the catalyst reaches 40.1%. As the copper content increases, the dispersion of copper continues to decrease. This is consistent with other characterization results (such as XRD, H_2-TPR). It suggests that the larger copper clusters may form as the copper content increases, which is not conducive to the dispersion of copper. Comparing the 12% Cu-ZrO_2 catalyst prepared under different calcination conditions, it is found that the 12% Cu-ZrO_2-1-3 catalyst has the highest copper dispersion (32.4%), which is 3.1% higher than that of the 12%

Table 3
Comparison of copper particles and structural feastures with other reported catalysts.

Catalysts	D_C(nm)	BET surface area (m^2 g^{-1})	Pore volume (cm^3 g^{-1})	Pore size (nm)	Ref
Pure CuO	140	42			[43]
Cu-ZrO_2-CeO_2(CZC35)	15.3	83	–	10	[44]
Cu-ZrO_2(DP3)	16	172			[43]
CuZnAlZr	6.5	68	–	–	[12]
CuZnZrGaY	9	125			[45]
Cu-ZrO_2	17.5	26.9	0.14	3.8	[46]
Cu-m-ZrO_2	7	111	0.23	–	[37]
Cu(4)-ZrO_2	37.9	4.2	2.5		[47]
12%Cu-ZrO_2-1-3	3.1	53	0.06	5.4	THIS WORK

Cu-ZrO_2 catalyst calcined in air alone. It shows that calcination in nitrogen improves the dispersion of copper. However, when the calcination time in nitrogen was changed to 3 h, the dispersion of copper dropped to 25.7%, indicating that extended calcination time in nitrogen is not conducive to copper dispersion. When comparing the 12%Cu-ZrO_2-1-3 catalyst with the control group (the 12%Cu-ZrO_2-im), copper dispersion of the 12%Cu-ZrO_2-1-3 is more than 4 times of that of 12%Cu-ZrO_2-im. This suggests that the preparation method can significantly improve the dispersion of copper.

BET surface areas show a similar trend with surface area reaching maximum at 12%Cu-ZrO_2-2–2 (67 m^2 g^{-1}). It indicates that calcination in nitrogen is helpful to form a catalyst with a high specific surface area. However, as the calcination time in nitrogen increases, the specific surface area also tends to decrease, which is consistent with the trend of copper dispersion.

The reason for the decreased copper dispersion for 12%Cu-ZrO_2-3-1 is analyzed by studying carbon content of these catalysts. Carbon content is determined by the combustion method and is shown in Table S8. According to the element analysis, it is concluded that carbon content of 12%Cu-ZrO_2-1-3 and 12%Cu-ZrO_2-2–2 is very low, while it is high for 12%Cu-ZrO_2-3-1 (1.47%). This shows that longer calcination time in nitrogen leads to the formation of more amorphous carbon that is difficult to be removed in the one-hour calcination in air. The presence of these carbon inhibits the activity of copper and covers a portion of the copper on the surface. Therefore, activity of the catalyst and the copper dispersion are reduced.

Table 3 summarizes some of the copper particles prepared and their surface information. The copper nanoclusters (3.1 nm) prepared in this research are competitive because of the smaller copper particle sizes.

To understand the reducibility of the catalysts, H_2-TPR analysis was performed. The low temperature peak (below 250 ℃) refers to the reduction of highly dispersed CuO nanoparticles supported on the ZrO_2 surface, while the high temperature peak (over 400 ℃) represents the reduction of larger agglomerated CuO particles [28]. The H_2-TPR profile reveals that all the reduced sites of the catalysts are within the low temperature region, which means that the CuO nanoparticles are well dispersed on the ZrO_2 surface. As shown in Fig. 4(a), with the increase of ZrO_2 content, the reducing temperature decreases. It suggests that the presence of ZrO_2 contributes to the reduction of CuO, which is consistent with previous findings [28]. When copper content reaches 42 wt%, some copper clusters aggregates to form larger copper particles, corresponding to the β peak in Fig. 4(a).

Fig. 4(b) shows the profile of 12% Cu-ZrO_2 catalysts calcined in nitrogen with different time. The 12% Cu-ZrO_2-1-3 catalyst exhibits the lowest reduction temperature, indicating the best dispersion of CuO. With the increase in calcination time in nitrogen, the reducing temperature of as-prepared catalysts reduced to 223 ℃ with 12%Cu-ZrO_2-1-3 before increasing significantly to 262 ℃ for 12% Cu-ZrO_2-3-1. It suggests that calcination in nitrogen can help improve copper dispersion

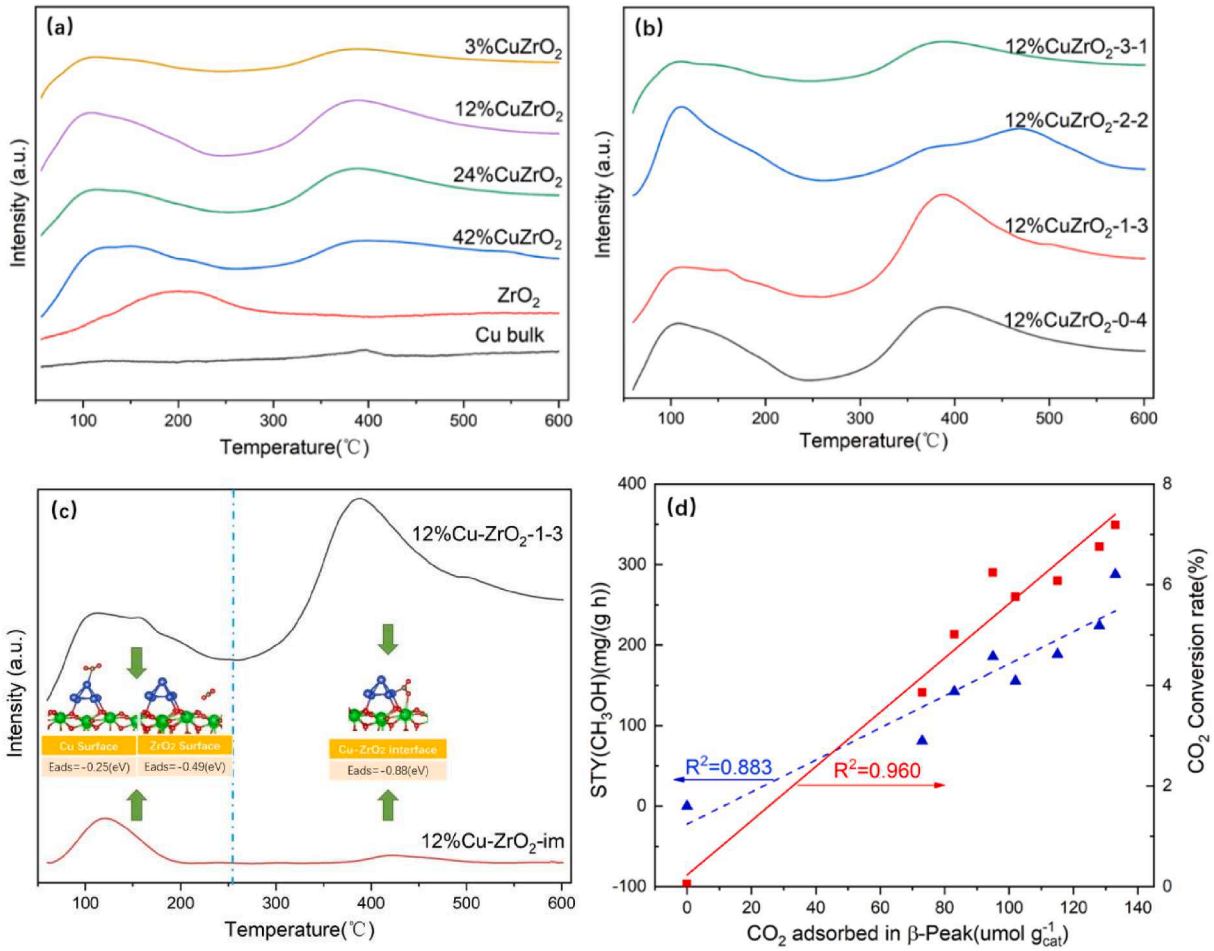

Fig. 5. CO_2 desorption profile of the catalysts with (a) the effect of Cu content; (b) the effect of calcination atmosphere; (c) the combination of DFT simulation with CO_2-TPD profile of 12%Cu-ZrO_2-1-3 and 12%Cu-ZrO_2-im; (d) the correlation between CO_2 adsorbed in β peak (strong sties) with CO_2 conversion and STY (CH_3OH).

because of the presence of carbon, which acts as a physical spacer. As shown in Fig. 4(b), a new β peak at 292 ℃ is detected alongside with the α peak in 12% Cu-ZrO_2-3-1, which can be attributed to copper that is not easily reduced (might be covered by carbon in 12% Cu-ZrO_2-3-1). Fig. S17 shows a comparison for 12%Cu-ZrO_2-1-3 with 12%Cu-ZrO_2-im. Compared with 12%Cu-ZrO_2-1-3, the TPR peak for 12%Cu-ZrO_2-im is wider and flatter. It indicates that a part of copper is difficult to be reduced because of forming larger partilcles.It suggests that the 12%Cu-ZrO_2-1-3 catalysts have more dispersed copper than 12%Cu-ZrO_2-im.

The reduction temperature during H_2-TPR, to a certain extent, reflect the degree of metal dispersion on the support [28]. Combining with the catalytic performance test as shown in Fig. 1, the catalyst with the best dispersion is also the one with the highest catalytic activity. This indicates that the dispersion of active sites has significant impacts on CO_2 hydrogenation.

The changes in valence state of copper for the 12% Cu-ZrO_2 catalysts by XPS analysis are shown in Fig. 4(c,d). Copper XPS spectra in Fig. 4(c) are used to analyze the presence of bivalent copper, while the Auger peaks of copper in Fig. 4(d) are used for qualitative analysis of the existence of univalent and zero-valent copper. The small peak appears at 933.8 eV in Fig. 4(c), suggesting that a small amount of Cu ions in the Cu-ZrO_2 catalyst are in a bivalent state [48,49]. It can be observed that the as-prepared catalysts exhibit the bonding signals of Cu^0 and Cu^+ species with bonding energy between 932.4 eV and 932.8 eV [50,51] in Fig. 4(c). However, it is difficult to distinguish the two valence states of copper because the positions are too close. Thus, Auger peaks of Cu are analyzed in Fig. 4(d) to explore the existence of Cu^+. There are obvious peaks at 916.7 eV (corresponding to Cu^+) for these three catalysts with different calcination times in nitrogen. However, the 12% Cu-ZrO_2-0–4 catalyst shows the peak at around 917.4 eV, which may be the result of the overlapping of the peak at 916.7 eV and at 918 eV (corresponding to Cu^0 [52–54]). This suggests that calcination in nitrogen helps produce Cu^+, and a similar result has been reported by other researchers [55]. It has been reported that Cu^+ can promote the conversion of carbon dioxide to methanol [56]. For the as-prepared catalysts, the bulging trend is observed at 918 eV for the 12% Cu-ZrO_2-1-3 and the 12% Cu-ZrO_2-2–2, whereas for the 12% Cu-ZrO_2-3-1 there is no such trend. It suggests that as nitrogen calcination time increases, Cu^0 decreases and the proportion of Cu^+ increases. Therefore, the 12% Cu-ZrO_2-1-3 may have the most suitable valence state of copper with the best copper dispersion.

3.3. The role of copper-zirconia interface

The larger copper-zirconia interface can contribute significantly to the catalytic performance in CO_2 hydrogenation process [34,38,57,58]. The interface of the as-prepared catalysts is analyzed by combing TPD results with DFT simulation.

Surface basicity of the calcined Cu-ZrO_2 catalysts was studied using CO_2-TPD as shown in Fig. 5. In all cases, active sites of the catalysts can be divided into two categories, weak (50–200 ℃) and strong (300–600 ℃) CO_2 adsorption sites. Bulk copper shows very low CO_2 adsorption at high-temperatures. ZrO_2 shows a relatively high ability to adsorb CO_2 at low temperatures. Surface basicity of Cu-ZrO_2 composites vary significantly depending on the wt% of copper (Fig. 5(a)) and calcination conditions (Fig. 5(b)). In Fig. 5(a), the 12%Cu-ZrO_2 shows best surface affinity to CO_2. Considering the 12% Cu-ZrO_2 showed the best catalytic

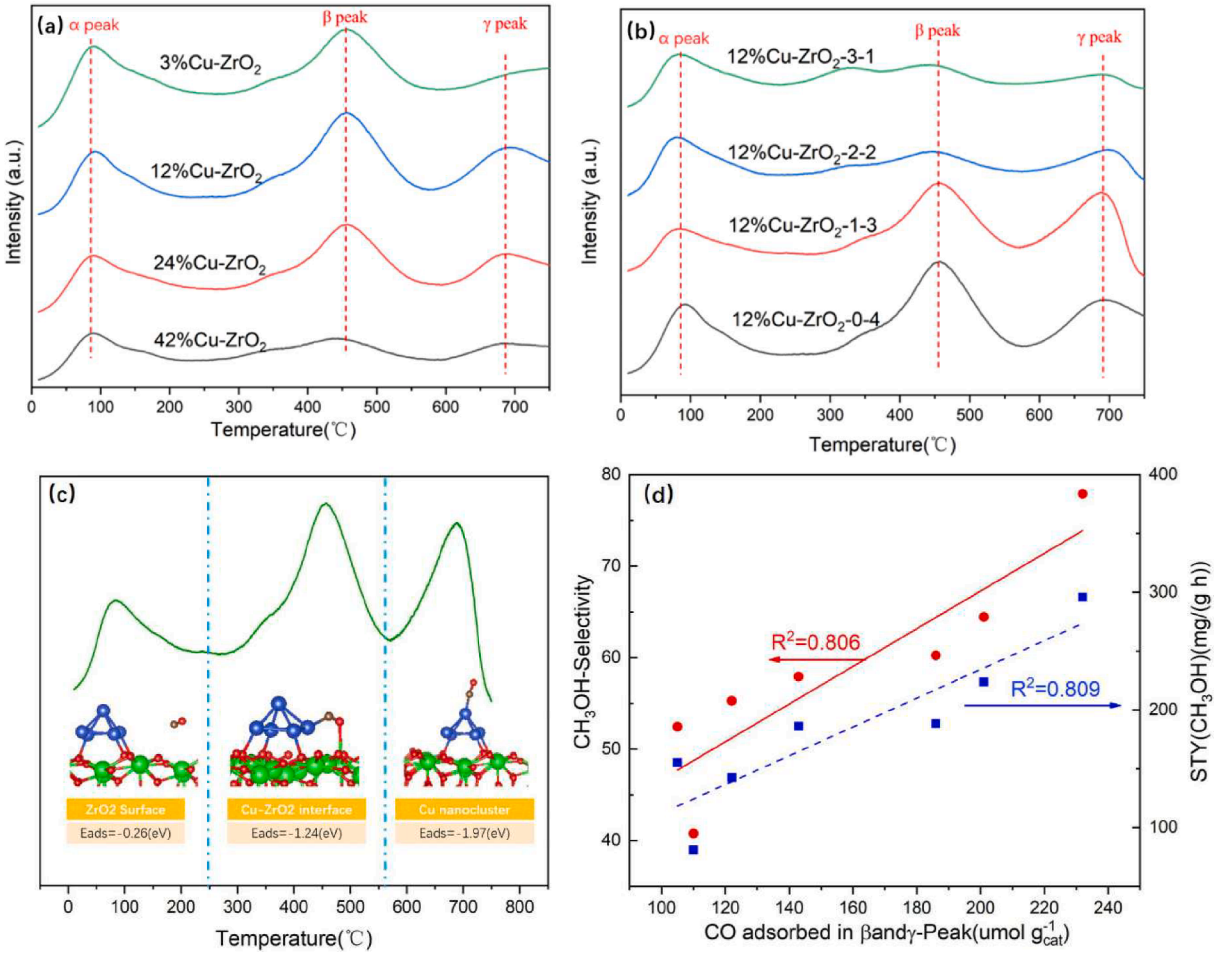

Fig. 6. CO desorption profile of catalysts with (a) different percentages of ZrO_2 (b) different times of calcination; (c) Combination of DFT simulation with CO-TPD profile of the 12% Cu-ZrO_2-1-3; (d) Correlation between CO adsorbed in β and γ peak with CH_3OH selectivity and STY (CH_3OH).

performance in Fig. 1(a), it suggests that the catalytic conversion of CO_2 is closely related to the amount of basic sites on the catalyst surface.

It is worth noting that calcination conditions can play a significant role in surface basicity. The CO_2 adsorption ability reaches the highest for the catalyst that is calcined in nitrogen for 1 h followed by in air for 3 h. This shows that calcination in nitrogen for 1 h could increase the basic sites on the surface. Combined with TGA analysis in Fig. S11, it suggests that when calcined in nitrogen, the carbon produced by the decomposition of HKUST-1 can be used as an effective physical barrier, to prevent copper from agglomeration before removal by calcination in air [59], resulting in the formation of highly dispersed copper-based catalysts. However, only calcination in nitrogen for an optimal period of time can improve the dispersion of copper. When the calcination time in nitrogen reaches 3 h, the dispersion of copper particles decreased (according to the copper dispersion results in Table 2 and H_2-TPR in Fig. 4), which explains why the 12% Cu-ZrO_2-1-3 produces the most amount of CO_2 adsorption sites and the highest catalytic performance.

DFT simulations were performed to further clarify the effect of low and high temperature active sites on catalytic activity. CO_2 adsorption energy on different sites of the Cu-ZrO_2 surface was calculated using VASP, which is shown in Fig. 5(c). Adsorption energies are used to determine the possibility of CO_2 desorption at various sites [60]. DFT calculations suggest that weak basic sites are associated with CO_2 adsorbed on copper surfaces (with adsorption energy of −0.25 eV) and on ZrO_2 surfaces (with adsorption energy of −0.49 eV), whereas the strong basic sites are closely related to the CO_2 adsorbed on the Cu-ZrO_2 interface(with adsorption energy of −0.88 eV). Comparing with the 12% Cu-ZrO_2-1-3 catalyst, the strong basic sites of the 12%Cu-ZrO_2-im is very limited. This suggests that there is only a very small amount of Cu-ZrO_2 interfaces in the 12%Cu-ZrO_2-im catalyst. This is because most of the copper is not dispersed on the surface of zirconia, but agglomerates to form large copper particles, which is consistent with the results of XRD and TPR analyses. The length of the carbon–oxygen bond shows the ability of the catalyst to activate carbon dioxide. The carbon–oxygen bond of CO_2 adsorbed on Cu surface changes from 1.176 Å to 1.179 Å and that on ZrO_2 surface changes from 1.176 Å to 1.184 Å. However, the carbon–oxygen bond changes significantly on the Cu-ZrO_2 interface, from 1.176 Å to 1.287 Å. These results confirm that only the Cu-ZrO_2 interface can effectively activate carbon dioxide. Therefore, the interface sites play a decisive role in the conversion of carbon dioxide, whereas weak adsorption sites, below the reaction temperature, have little contribution to the catalytic reaction as well as the activation of CO_2.

The relationship is further verified by the experimental results, as illustrated in Fig. 5(d), which shows the correlation between the CO_2 adsorption, CO_2 conversion and space time yield of methanol (denoted as STY(CH_3OH)). The data used in Fig. 5(d) were calculated based on the CO_2-TPD profile of this series of Cu-ZrO_2 catalysts. The increase in CO_2 adsorbed at strong adsorption sites can be attributed to the larger Cu-ZrO_2 interface, which leads to more CO_2 being activated, resulting in a higher CO_2 conversion and a potentially larger space time yield of methanol. A linear relationship is obtained with R^2 as 0.960 for CO_2 conversion, indicating that CO_2 conversion rate is strongly related to the CO_2 adsorbed at strong adsorption sites. However, the correlation between CO_2 adsorption and STY of methanol shows a weaker correlation with a coefficient of 0.883, implying that CO_2 activation is not the only

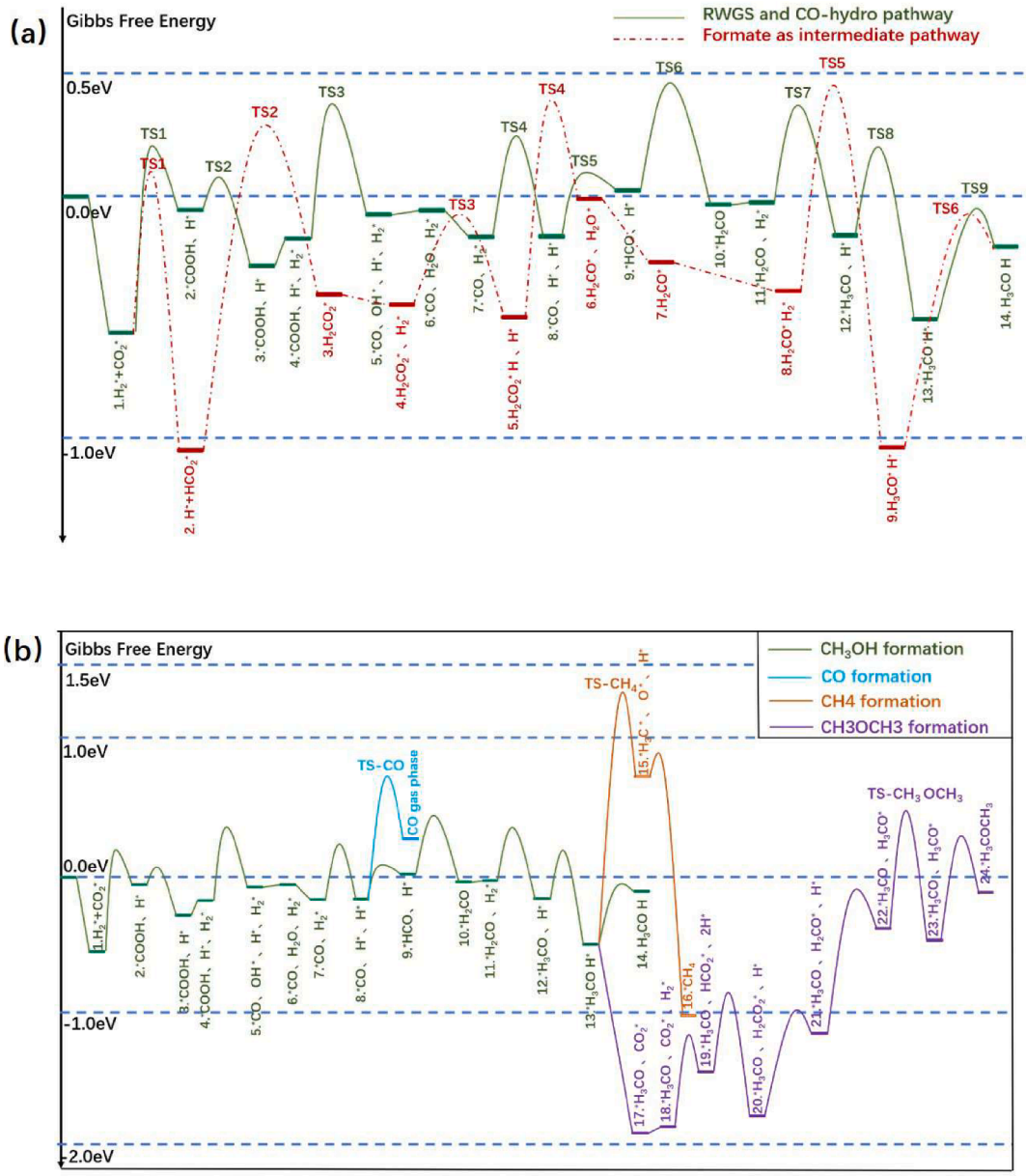

Fig. 7. (a) Gibbs Free Energy at 493.15 K for CO_2 hydrogenation to methanol on a Cu-ZrO_2 surface via two mechanistic pathways including methanol formation from CO (solid line) and formate as intermediates (dotted line); and (b) Formation pathway of by-product for CO_2 hydrogenation to methanol.

factor that affects methanol producibility. Unlike CO_2 conversion, the methanol producibility is affected by many other factors, such as selectivity to methanol and hydrogen activation. Therefore, it is difficult to find a single factor that dictates the production of methanol, but it is speculated that CO_2 adsorption at intermediate and high temperature sites is positively correlated with methanol production rates.

As the main by-product in the CO_2 hydrogenation process, the surface affinity of CO and CO adsorption sites on the as-prepared catalysts were studied using CO-TPD and DFT simulation. There are three peaks for the Cu-ZrO_2 catalysts depending on copper content (Fig. 6(a)) and the calcination method (Fig. 6(b)). The amount of adsorbed CO in each peak is shown in Table S5. Combining the results from DFT study (Fig. 6 (c)), the first peak (denoted as α peak) occurs at low temperatures ranging from 50 to 250℃ and is attributed to the adsorption of carbon monoxide on ZrO_2 surface with an adsorption energy of −0.26 eV. The second peak (denoted as β peak) occurs at a medium temperature range (250 to 550 ℃) and is associated with CO adsorption on Cu-ZrO_2 interface with a medium adsorption energy of −1.24 eV. The third peak (denoted as γ peak) is found at high temperatures from 550 to 750 ℃, and assigned to adsorption sites on the copper surface with an adsorption energy of −1.97 eV. The production of CO is closely related to the binding ability of the surface. When the surface has more strong adsorption sites for CO, the *CO (adsorbed CO) tends to hydrogenate or dissociate instead of desorbing [61], thereby leading to a low level of CO desorption and a higher selectivity towards methanol. As shown in Fig. 6 (c), the medium and strong adsorption sites tend to form strong chemical bonds with carbon monoxide. Therefore, the highest methanol selectivity is achieved for the catalyst with the most medium and strong adsorption sites for CO. From the data in Fig. 6(a), these sites are optimal when the Cu-ZrO_2 catalyst with 12 wt% of Cu. The calcination method is optimal for the 12% Cu-ZrO_2-1-3 catalyst (Fig. 6(b)), which shows the highest CO adsorption at β and γ peaks. These results are consistent with the catalytic performance shown in Fig. 1(b).

The correlation was conducted in Fig. 6(d) to better understand the role of CO adsorption sites. A relationship is obtained with R^2 as 0.806 for CH_3OH selectivity and 0.809 for methanol production. Similar as

Table 4
The adsorption energy of products involved in CO_2 hydrogenation process (Unit: eV).

Sites	H_2	CO_2	CO	CH_2O	CH_3OH	CH_4	CH_3OCH_3
On Cu surface	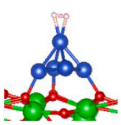 Eads=-0.80	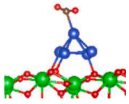 Eads=-0.25	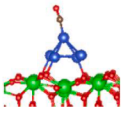 Eads=-1.97	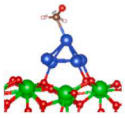 **Eads=-0.50**	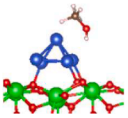 Eads=-0.32	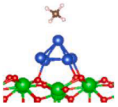 Eads=0.86	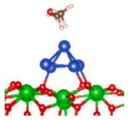 Eads= 2.78
On Cu-ZrO_2 interface	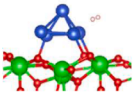 Eads=-0.22	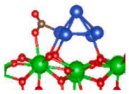 Eads= -0.88	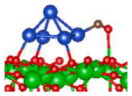 Eads= -1.24	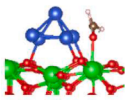 **Eads= -1.31**	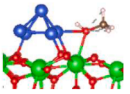 Eads= -0.71	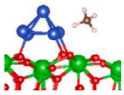 Eads= 0.91	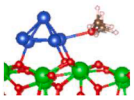 Eads= 2.49
On ZrO_2 surface	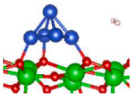 Eads=-0.28	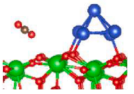 Eads= -0.49	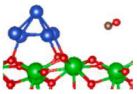 Eads= -0.26	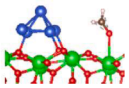 Eads= -0.58	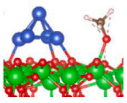 Eads= -0.69	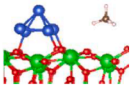 Eads=0.99	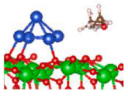 Eads= 2.55

Fig. 5(d), It suggests that other factors (beyond CO adsorption sites) also play a role in CH_3OH selectivity. From the analysis of by-product, as shown in Fig. 1(c) and the by-product energy barrier simulation, as shown in Fig. 7(b), carbon monoxide is not the only by-product. The production of dimethyl ether and methane could also significantly affect the selectivity of methanol.

In order to further understand the role of the Cu-ZrO_2 interface in the whole reaction process, the adsorption energy for the reactants, products and by-products on different positions of the Cu-ZrO_2 surface are shown in Table 4. Generally, the more negative the adsorption energy value, the stronger the adsorption between the adsorbed species and the support. For methane and DME, the value of the adsorption energy is positive, indicating that the surface cannot adsorb these two species. Once these two by-products are generated on the catalyst surface, they are desorbed immediately and no longer occupy active sites. The ability to fix and activate the reactant(s) and possible intermediates is the key to further hydrogenation reactions. It can be seen from Table 4 that the large copper-zirconia interface could strongly adsorb carbon dioxide, carbon monoxide and formaldehyde, which is beneficial for further hydrogenation reactions, and thus result in high methanol selectivity.

3.4. Possible reaction pathways

The intermediate that contributes the most to the formation of methanol has been somewhat controversial [62–64]. Thereby, DFT calculations were performed to explore the reaction pathways during CO_2 hydrogenation. Herein, the Cu-ZrO_2 catalysts were modeled by depositing a small Cu cluster on the ZrO_2(−1 1 1) surface (details are available in Supporting information in Fig. S3). Some researchers have studied the hydrogenation mechanism using a similar model [32,63]. Herein, the two possible pathways are simulated using the same model for discussion: one is the reverse water–gas (RWGS) and CO as intermediate pathway, the other is the use of formates as an intermediate pathway. Both are simulated in Fig. 7(a).

3.4.1. Gibbs Free energy of the two potential pathways

The Gibbs Free Energy of the two pathways is shown in Fig. 7(a). The detailed structures and reaction pathways of relative energy are illustrated in Figs. S5 and S6. The reaction starts with the co-adsorption of carbon dioxide and hydrogen with an adsorption energy of −0.66 eV. The next step is the divergence of the two pathways:

CO_2 transformed to:

- Carboxyl intermediate (COOH*, solid line in Fig. 7(a))
- Formate intermediate (HCOO*, dotted line in Fig. 7(a)).

It is obvious that the activation barrier to form formate (ΔG = 0.77 eV) is slightly lower than that for the formation of carboxyl (ΔG = 0.87 eV) intermediate (from Step 1 to TS1). Thermodynamically, the favorable pathway is also the formate as intermediate (-1.02 eV) compared with the formation of a carboxyl (-0.07 eV). This trend is consistent with another researcher [62]. However, the CO_2 transformation step is just the first step. When comparing the reaction speed, the rate-limiting step of the entire reaction pathway should be considered. According to Murdoch's literature [65], the rate-limiting step was determined from the step with the lowest energy to the highest TS stage. In Fig. 7(a), the rate-limiting step of carboxyl intermediate pathway (solid line) was from Step 1 to TS6 with an activation energy of 1.11 eV whereas the activation energy for formate pathway(dotted line) was 1.46 eV (from Step 2 to TS5). The reaction rate constants (k) were calculated using the Eyring equation (Eq. (4)). At the reaction conditions, the reaction rate constant (k) for carboxyl pathway is 51 s^{-1}, which is much more favorable than the formate pathway with a reaction rate constant (k) of 0.014 s^{-1}. These results are consistent with Kattel's work [66], using experimental in-Situ DRIFTS to confirm that the formate route was unfevorable. As a result, both intermediates, carboxyl and formate could be produced in the reaction pathway, but the reaction speed of RWGS and methanol formation from CO pathway is faster.

The possible RWGS and methanol formation from CO pathway is:

RWGS follows: $CO_2{}^* + H_2{}^* \rightarrow COOH^* + H^* \rightarrow CO^* + H_2O$ (R6)

Methanol formation from CO: $CO^*+2H_2^*\rightarrow *HCO + H^*+H_2^*\rightarrow *CH_2O + H_2^*\rightarrow *CH_3O + H^*\rightarrow CH_3OH$ (R7)

3.4.2. Formation of by-products

Researchers have pointed out that methanol selectivity decreased significantly when the reaction temperature is high [29]. But the pathway of each by-product has seldom been studied. The Gibbs free energy of the formation of each by-product is discussed and shown in Fig. 7(b).

At all reaction temperatures CO is the major by-product (Fig. 1(c)), suggesting that the desorption of CO is critical to the selectivity of the reaction. Thus, the product selectivity is mainly determined by the competition between CO desorption and the hydrogenation reaction. The selectivity controlling step is shown in Fig. 7(b) between CO further hydrogenation (Step 8 to Step 9 in green) and CO desorption (blue line). The activation energy of CO desorbing from the Cu-ZrO_2 surface is 0.95 eV at 493.15 k, which is much higher than that for further hydrogenation (0.36 eV) to methanol. This suggests that CO prefers further hydrogenation instead of desorbing, accounting for the high selectivity in CO_2 catalytic reaction. The reaction pathways of the other by-products are also simulated and shown in Fig. 7(b) (orange line for methane and purple line for DME). It is clear that the activation energy to produce methane and DME are rather high compared to that for methanol and carbon monoxide. The rate-limiting step of methane formation is from Step 1 to TS-CH_4 with an activation energy of 2.07 eV. According to the Eyring equation, the reaction rate constant (k) for methane formation at 493.15 k is $7.51\cdot10^{-9}$ s^{-1}. The rate is very slow, making it virtually impossible to produce methane, which would be consistent with the very low percentage seen in the by-product.

4. Conclusions

In short, this study revealed that the pyrolysis of HKUST-1 can lead to a higher dispersion of copper nano-clusters and a larger Cu-ZrO_2 interfacial area than the traditional impregnation method. The main results are summarized as follows:

- We demonstrated the possibility of using the ZrO_2/HKUST-1 composites as an adjustable template to fabricate Cu-ZrO_2 catalysts with highly dispersed Cu nanoclusters and show a promising catalytic performance in CO_2 hydrogenation.
- The 12 wt% Cu-ZrO_2-1-3 was confirmed to be the best performing catalyst with a 5.2 times higher methanol production rate.
- The active sites were investigated by combining experimental results with a DFT study, which showed that the Cu-ZrO_2 interface not only activates carbon dioxide, but also stabilizes the intermediates such as carbon monoxide and fomaldehyde, indicating that the interface plays an essential role in the conversion of carbon dioxide as well as the selective formation of methanol.

Declaration of Competing Interest

The authors declare that they have no known competing financial interests or personal relationships that could have appeared to influence the work reported in this paper.

Acknowledgement

This research is partially sponsored by Ningbo Science and Technologies Innovation 2025 Major Special Project (2018B10027). The Zhejiang Provincial Department of Science and Technology is acknowledged for its financial support to the Provincial Key Laboratory (2020E10018). Ningbo Bureau of Science and Technology is also thanked for its support to the Key Laboratory of Clean Energy Conversion Technologies, while Ningbo Bureau of Education is acknowledged for awarding the Municipal Collaborative Innovation Centre for Carbonaceous Wastes and Processing Intensification. The University of Nottingham Ningbo China provides full scholarships to the first two authors.

Appendix A. Supplementary data

Supplementary data to this article can be found online at https://doi.org/10.1016/j.cej.2021.129656.

References

[1] M. Bertau, et al., Methanol: the basic chemical and energy feedstock of the future. 2014: Springer.
[2] L. Yuan, Y.-J. Xu, Photocatalytic conversion of CO2 into value-added and renewable fuels, Appl. Surf. Sci. 342 (2015) 154–167.
[3] S. Kuld, M. Thorhauge, H. Falsig, C.F. Elkjaer, S. Helveg, I. Chorkendorff, J. Sehested, Quantifying the promotion of Cu catalysts by ZnO for methanol synthesis, Science 352 (6288) (2016) 969–974.
[4] T. Phongamwong, U. Chantaprasertporn, T. Witoon, T. Numpilai, Y. Poo-arporn, W. Limphirat, W. Donphai, P. Dittanet, M. Chareonpanich, J. Limtrakul, CO2 hydrogenation to methanol over CuO–ZnO–ZrO2–SiO2 catalysts: effects of SiO2 contents, Chem. Eng. J. 316 (2017) 692–703.
[5] X. Cui, S.K. Kær, A comparative study on three reactor types for methanol synthesis from syngas and CO2, Chem. Eng. J. 393 (2020) 124632, https://doi.org/10.1016/j.cej.2020.124632.
[6] E. Lam, K. Larmier, P. Wolf, S. Tada, O.V. Safonova, C. Copéret, Isolated Zr surface sites on silica promote hydrogenation of CO2 to CH3OH in supported Cu catalysts, J. Am. Chem. Soc. 140 (33) (2018) 10530–10535.
[7] J.-Y. Li, L. Yuan, S.-H. Li, Z.-R. Tang, Y.-J. Xu, One-dimensional copper-based heterostructures toward photo-driven reduction of CO2 to sustainable fuels and feedstocks, J. Mater. Chem. A 7 (15) (2019) 8676–8689.
[8] L. Zheng, X. Li, W. Du, D. Shi, W. Ning, X. Lu, Z. Hou, Metal-organic framework derived Cu/ZnO catalysts for continuous hydrogenolysis of glycerol, Appl. Catal. B 203 (2017) 146–153.
[9] Z. Yuan, L. Wang, J. Wang, S. Xia, P. Chen, Z. Hou, X. Zheng, Hydrogenolysis of glycerol over homogenously dispersed copper on solid base catalysts, Appl. Catal. B 101 (3-4) (2011) 431–440.
[10] C. Huang, J. Wen, Y. Sun, M. Zhang, Y. Bao, Y. Zhang, L. Liang, M. Fu, J. Wu, D. Ye, L. Chen, CO2 hydrogenation to methanol over Cu/ZnO plate model catalyst: Effects of reducing gas induced Cu nanoparticle morphology, Chem. Eng. J. 374 (2019) 221–230.
[11] Q. Quan, et al., Photoelectrochemical reduction of CO2 over graphene-based composites: basic principle, recent progress, and future perspective, Acta Phys. Chim. Sin. 33 (12) (2017) 2404–2423.
[12] S. Xiao, Y. Zhang, P. Gao, L. Zhong, X. Li, Z. Zhang, H. Wang, W. Wei, Y. Sun, Highly efficient Cu-based catalysts via hydrotalcite-like precursors for CO2 hydrogenation to methanol, Catal. Today 281 (2017) 327–336.
[13] F.-W. Chang, W.-Y. Kuo, K.-C. Lee, Dehydrogenation of ethanol over copper catalysts on rice husk ash prepared by incipient wetness impregnation, Appl. Catal. A 246 (2) (2003) 253–264.
[14] T. Whittaker, K.B.S. Kumar, C. Peterson, M.N. Pollock, L.C. Grabow, B.D. Chandler, H2 oxidation over supported Au nanoparticle catalysts: evidence for heterolytic H2 activation at the metal–support interface, J. Am. Chem. Soc. 140 (48) (2018) 16469–16487.
[15] L. Peng, X. Zheng, L.i. Li, L. Zhang, N.a. Yang, K. Xiong, H. Chen, J. Li, Z. Wei, Chimney effect of the interface in metal oxide/metal composite catalysts on the hydrogen evolution reaction, Appl. Catal. B 245 (2019) 122–129.
[16] X. Yang, X. Yu, M. Lin, M. Ge, Y. Zhao, F. Wang, Interface effect of mixed phase Pt/ZrO2 catalysts for HCHO oxidation at ambient temperature, J. Mater. Chem. A 5 (26) (2017) 13799–13806.
[17] X. Yang, S. Kattel, S.D. Senanayake, J.A. Boscoboinik, X. Nie, J. Graciani, J. A. Rodriguez, P. Liu, D.J. Stacchiola, J.G. Chen, Low Pressure CO2 Hydrogenation to Methanol over Gold Nanoparticles Activated on a CeO x/TiO2 Interface, J. Am. Chem. Soc. 137 (32) (2015) 10104–10107.
[18] E. Lam, J.J. Corral-Pérez, K. Larmier, G. Noh, P. Wolf, A. Comas-Vives, A. Urakawa, C. Copéret, CO2 hydrogenation on Cu/Al2O3: Role of the metal/support interface in driving activity and selectivity of a bifunctional catalyst, Angew. Chem. 131 (39) (2019) 14127–14134.
[19] A. Le Valant, C. Comminges, C. Tisseraud, C. Canaff, L. Pinard, Y. Pouilloux, The Cu–ZnO synergy in methanol synthesis from CO2, Part 1: Origin of active site explained by experimental studies and a sphere contact quantification model on Cu +ZnO mechanical mixtures, J. Catal. 324 (2015) 41–49.
[20] G. Lu, S. Li, Z. Guo, O.K. Farha, B.G. Hauser, X. Qi, Y.i. Wang, X. Wang, S. Han, X. Liu, J.S. DuChene, H. Zhang, Q. Zhang, X. Chen, J. Ma, S.C.J. Loo, W.D. Wei, Y. Yang, J.T. Hupp, F. Huo, Imparting functionality to a metal–organic framework material by controlled nanoparticle encapsulation, Nat. Chem. 4 (4) (2012) 310–316.
[21] Y. Chen, X. Mu, E. Lester, T. Wu, High efficiency synthesis of HKUST-1 under mild conditions with high BET surface area and CO2 uptake capacity, Progress in Natural Science: Materials International 28 (5) (2018) 584–589.

[22] X. Mu, Y. Chen, E. Lester, T. Wu, Optimized synthesis of nano-scale high quality HKUST-1 under mild conditions and its application in CO2 capture, Microporous Mesoporous Mater. 270 (2018) 249–257.

[23] G. Yang, H. Zhao, X. Luo, K. Shi, H. Zhao, W. Wang, Q. Chen, H. Fan, T. Wu, Promotion effect and mechanism of the addition of Mo on the enhanced low temperature SCR of NOx by NH3 over MnOx/γ-Al2O3 catalysts, Appl. Catal. B 245 (2019) 743–752.

[24] C.J.G. Van Der Grift, et al., Effect of the reduction treatment on the structure and reactivity of silica-supported copper particles, J. Catal. 131 (1) (1991) 178–189.

[25] L. Yuan, et al., Unveiling the interplay between light-driven CO2 photocatalytic reduction and carbonaceous residues decomposition: A case study of Bi2WO6-TiO2 binanosheets, Appl. Catal. B 237 (2018) 424–431.

[26] B.S. Kulkarni, S. Krishnamurty, S. Pal, Influence of plane wave cut-off on structural and electronic properties in Sn-BEA and Ti-BEA zeolite water molecule interaction, Chem. Phys. Lett. 484 (4-6) (2010) 374–379.

[27] Wang, V., et al., VASPKIT: A Pre-and Post-Processing Program for VASP code. arXiv preprint arXiv:1908.08269, 2019.

[28] C. Zhong, X. Guo, D. Mao, S. Wang, G. Wu, G. Lu, Effects of alkaline-earth oxides on the performance of a CuO–ZrO2 catalyst for methanol synthesis via CO2 hydrogenation, RSC Adv. 5 (65) (2015) 52958–52965.

[29] D. Chen, D. Mao, G. Wang, X. Guo, J. Yu, CO2 hydrogenation to methanol over CuO-ZnO-ZrO2 catalyst prepared by polymeric precursor method, J. Sol-Gel Sci. Technol. 89 (3) (2019) 686–699.

[30] J. Wang, G. Li, Z. Li, C. Tang, Z. Feng, H. An, H. Liu, T. Liu, C. Li, A highly selective and stable ZnO-ZrO2 solid solution catalyst for CO2 hydrogenation to methanol, Sci. Adv. 3 (10) (2017) e1701290, https://doi.org/10.1126/sciadv.1701290.

[31] Q. Tan, Z. Shi, D. Wu, CO2 Hydrogenation to Methanol over a Highly Active Cu-Ni/CeO2-Nanotube Catalyst, Ind. Eng. Chem. Res. 57 (31) (2018) 10148–10158.

[32] Y. Wang, S. Kattel, W. Gao, K. Li, P. Liu, J.G. Chen, H. Wang, Exploring the ternary interactions in Cu-ZnO-ZrO2 catalysts for efficient CO2 hydrogenation to methanol, Nat Commun 10 (1) (2019), https://doi.org/10.1038/s41467-019-09072-6.

[33] Y. Sun, L. Chen, Y. Bao, G. Wang, Y. Zhang, M. Fu, J. Wu, D. Ye, Roles of nitrogen species on nitrogen-doped CNTs supported Cu-ZrO2 system for carbon dioxide hydrogenation to methanol, Catal. Today 307 (2018) 212–223.

[34] K. Chen, et al., CO2 hydrogenation to methanol over Cu catalysts supported on La-modified SBA-15: The crucial role of Cu–LaOx interfaces, Appl. Catal. B 251 (2019) 119–129.

[35] H. Ren, C.-H. Xu, H.-Y. Zhao, Y.-X. Wang, J. Liu, J.-Y. Liu, Methanol synthesis from CO2 hydrogenation over Cu/γ-Al2O3 catalysts modified by ZnO, ZrO2 and MgO, J. Ind. Eng. Chem. 28 (2015) 261–267.

[36] J. Wang, C. Tang, G. Li, Z. Han, Z. Li, H. Liu, F. Cheng, C. Li, High-Performance MaZrOx (Ma = Cd, Ga) Solid-Solution Catalysts for CO2 Hydrogenation to Methanol, ACS Catal. 9 (11) (2019) 10253–10259.

[37] T. Witoon, J. Chalorngtham, P. Dumrongbunditkul, M. Chareonpanich, J. Limtrakul, CO2 hydrogenation to methanol over Cu/ZrO2 catalysts: Effects of zirconia phases, Chem. Eng. J. 293 (2016) 327–336.

[38] X. Dong, F. Li, N. Zhao, F. Xiao, J. Wang, Y. Tan, CO2 hydrogenation to methanol over Cu/ZnO/ZrO2 catalysts prepared by precipitation-reduction method, Appl. Catal. B 191 (2016) 8–17.

[39] F. ARENA, K. BARBERA, G. ITALIANO, G. BONURA, L. SPADARO, F. FRUSTERI, Synthesis, characterization and activity pattern of Cu–ZnO/ZrO2 catalysts in the hydrogenation of carbon dioxide to methanol, J. Catal. 249 (2) (2007) 185–194.

[40] J.H. Kwak, L. Kovarik, J. Szanyi, CO2 Reduction on Supported Ru/Al2O3 Catalysts: Cluster Size Dependence of Product Selectivity, ACS Catal. 3 (11) (2013) 2449–2455.

[41] R. Ye, A.V. Zhukhovitskiy, C.V. Deraedt, F.D. Toste, G.A. Somorjai, Supported Dendrimer-Encapsulated Metal Clusters: Toward Heterogenizing Homogeneous Catalysts, Acc Chem Res 50 (8) (2017) 1894–1901.

[42] Lu, K.-Q., et al., Rationally designed transition metal hydroxide nanosheet arrays on graphene for artificial CO 2 reduction.

[43] J. Liu, J. Shi, D. He, Q. Zhang, X. Wu, Y.u. Liang, Q. Zhu, Surface active structure of ultra-fine Cu/ZrO2 catalysts used for the CO2+ H2 to methanol reaction, Appl. Catal. A 218 (1-2) (2001) 113–119.

[44] A. Mastalir, et al., Steam reforming of methanol over Cu/ZrO2/CeO2 catalysts: a kinetic study, J. Catal. 230 (2) (2005) 464–475.

[45] S. Natesakhawat, J.W. Lekse, J.P. Baltrus, P.R. Ohodnicki, B.H. Howard, X. Deng, C. Matranga, Active sites and structure–activity relationships of copper-based catalysts for carbon dioxide hydrogenation to methanol, ACS Catal. 2 (8) (2012) 1667–1676.

[46] W. Wang, Z. Qu, L. Song, Q. Fu, CO2 hydrogenation to methanol over Cu/CeO2 and Cu/ZrO2 catalysts: Tuning methanol selectivity via metal-support interaction, Journal of Energy Chemistry 40 (2020) 22–30.

[47] H. Yin, C. Zhang, H. Yin, D. Gao, L. Shen, A. Wang, Hydrothermal conversion of glycerol to lactic acid catalyzed by Cu/hydroxyapatite, Cu/MgO, and Cu/ZrO2 and reaction kinetics, Chem. Eng. J. 288 (2016) 332–343.

[48] T. Ghodselahi, M.A. Vesaghi, A. Shafiekhani, A. Baghizadeh, M. Lameii, XPS study of the Cu@Cu2O core-shell nanoparticles, Appl. Surf. Sci. 255 (5) (2008) 2730–2734.

[49] A. Kumar, A. Singh, A.K. Debnath, S. Samanta, D.K. Aswal, S.K. Gupta, J. V. Yakhmi, Room temperature ppb level Cl2 sensing using sulphonated copper phthalocyanine films, Talanta 82 (4) (2010) 1485–1489.

[50] T.M. Ivanova, K.I. Maslakov, A.A. Sidorov, M.A. Kiskin, R.V. Linko, S.V. Savilov, V. V. Lunin, I.L. Eremenko, XPS detection of unusual Cu(II) to Cu(I) transition on the surface of complexes with redox-active ligands, J. Electron Spectrosc. Relat. Phenom. 238 (2020) 146878, https://doi.org/10.1016/j.elspec.2019.06.010.

[51] Kotwica, T., et al., Analysis of surface properties of Ti-Cu-Ox gradient thin films using AFM and XPS investigations. Materials Science-Poland, 2018. 36(4): p. 761-768.

[52] Zhang, B., et al., Effect of copper loading on texture, structure and catalytic performance of Cu/SiO2 catalyst for hydrogenation of dimethyl oxalate to ethylene glycol. Journal of natural gas chemistry, 2012. 21(5): p. 563-570.

[53] Z. Xie, B. Chen, H. Wu, M. Liu, H. Liu, J. Zhang, G. Yang, B. Han, Highly efficient hydrogenation of levulinic acid into 2-methyltetrahydrofuran over Ni–Cu/Al2O3–ZrO2 bifunctional catalysts, Green Chem. 21 (3) (2019) 606–613.

[54] X. Gong, M. Wang, H. Fang, X. Qian, L. Ye, X. Duan, Y. Yuan, Copper nanoparticles socketed in situ into copper phyllosilicate nanotubes with enhanced performance for chemoselective hydrogenation of esters, Chem. Commun. 53 (51) (2017) 6933–6936.

[55] L. Wang, X. Wang, Z. Meng, H. Hou, B. Chen, MOF-templated thermolysis for porous CuO/Cu2O@CeO2 anode material of lithium-ion batteries with high rate performance, J. Mater. Sci. 52 (12) (2017) 7140–7148.

[56] V.D.B.C. Dasireddy, B. Likozar, The role of copper oxidation state in Cu/ZnO/Al2O3 catalysts in CO2 hydrogenation and methanol productivity, Renewable Energy 140 (2019) 452–460.

[57] I. Ro, Y. Liu, M.R. Ball, D.H.K. Jackson, J.P. Chada, C. Sener, T.F. Kuech, R. J. Madon, G.W. Huber, J.A. Dumesic, Role of the Cu-ZrO2 interfacial sites for conversion of ethanol to ethyl acetate and synthesis of methanol from CO2 and H2, ACS Catal. 6 (10) (2016) 7040–7050.

[58] S. Tada, K. Fujiwara, T. Yamamura, M. Nishijima, S. Uchida, R. Kikuchi, Flame spray pyrolysis makes highly loaded Cu nanoparticles on ZrO2 for CO2-to-methanol hydrogenation, Chem. Eng. J. 381 (2020) 122750, https://doi.org/10.1016/j.cej.2019.122750.

[59] R. Zhang, L. Hu, S. Bao, R. Li, L. Gao, R. Li, Q. Chen, Surface polarization enhancement: high catalytic performance of Cu/CuOx/C nanocomposites derived from Cu-BTC for CO oxidation, J. Mater. Chem. A 4 (21) (2016) 8412–8420.

[60] A. Karelovic, P. Ruiz, The role of copper particle size in low pressure methanol synthesis via CO 2 hydrogenation over Cu/ZnO catalysts, Catal. Sci. Technol. 5 (2) (2015) 869–881.

[61] W. Li, G. Zhang, X. Jiang, Y.i. Liu, J. Zhu, F. Ding, Z. Liu, X. Guo, C. Song, CO2 Hydrogenation on Unpromoted and M-Promoted Co/TiO2 Catalysts (M = Zr, K, Cs): Effects of Crystal Phase of Supports and Metal-Support Interaction on Tuning Product Distribution, ACS Catal. 9 (4) (2019) 2739–2751.

[62] S. Kattel, B. Yan, Y. Yang, J.G. Chen, P. Liu, Optimizing Binding Energies of Key Intermediates for CO2 Hydrogenation to Methanol over Oxide-Supported Copper, J Am Chem Soc 138 (38) (2016) 12440–12450.

[63] K. Larmier, W.-C. Liao, S. Tada, E. Lam, R. Verel, A. Bansode, A. Urakawa, A. Comas-Vives, C. Copéret, CO2 -to-Methanol Hydrogenation on Zirconia-Supported Copper Nanoparticles: Reaction Intermediates and the Role of the Metal-Support Interface, Angew Chem Int Ed Engl 56 (9) (2017) 2318–2323.

[64] S. Kar, R. Sen, J. Kothandaraman, A. Goeppert, R. Chowdhury, S.B. Munoz, R. Haiges, G.K.S. Prakash, Mechanistic insights into ruthenium-pincer-catalyzed amine-assisted homogeneous hydrogenation of CO2 to methanol, J. Am. Chem. Soc. 141 (7) (2019) 3160–3170.

[65] Murdoch, J.R., What is the rate-limiting step of a multistep reaction? Journal of Chemical Education, 1981. 58(1): p. 32-32.

[66] S. Kattel, P. Liu, J.G. Chen, Tuning Selectivity of CO2 Hydrogenation Reactions at the Metal/Oxide Interface, J Am Chem Soc 139 (29) (2017) 9739–9754.